iScience

CellPress
OPEN ACCESS

Article

Arched microfluidic channel for the promotion of axonal growth performance

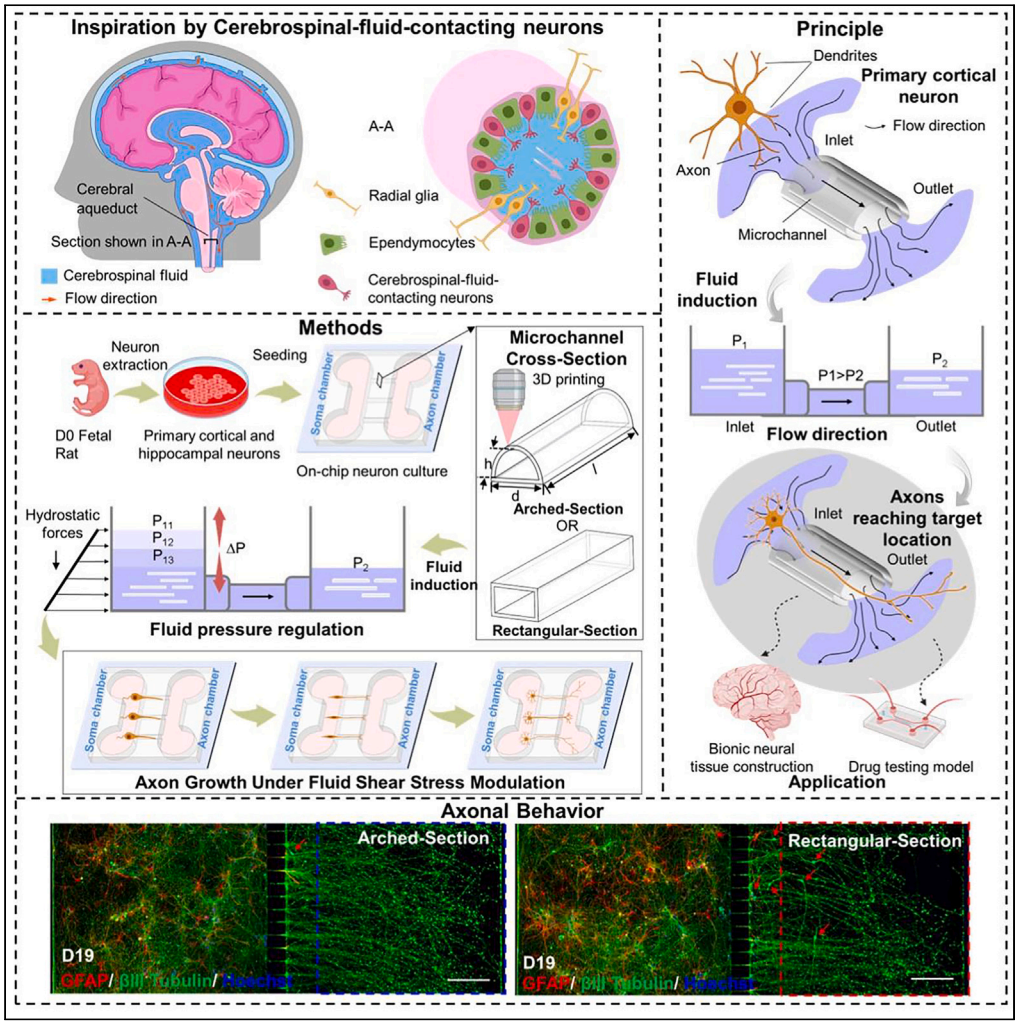

Menghua Liu, Anping Wu, Jiaxin Liu, ..., Qing Shi, Qiang Huang, Huaping Wang

wanghuaping@bit.edu.cn

Highlights

Design of channels inspired by the environment of cerebrospinal-fluid-contacting neurons

Arched-section microfluidic channels construct a uniform-stress-distributed environment

Changes in microfluidic channel configuration and pressure promote axonal performance

Microfluidic channel configuration and pressure guide neuronal axon redirection

Liu et al., iScience 27, 110885
October 18, 2024
https://doi.org/10.1016/j.isci.2024.110885

iScience

CellPress
OPEN ACCESS

Article

Arched microfluidic channel for the promotion of axonal growth performance

Menghua Liu,[1] Anping Wu,[1] Jiaxin Liu,[1] Hen-Wei Huang,[2] Yang Li,[3] Qing Shi,[4] Qiang Huang,[4] and Huaping Wang[5,6,*]

SUMMARY

Uniformly distributed fluid shear stress can promote axonal growth, aiding in the efficient construction of functional neural interfaces. However, challenges remain in the construction of the micro-scale environment with a uniform fluidic stress distribution. In this study, we designed and fabricated a microfluidic chip with arched-section microfluidic channels (AMCs) to increase primary cortical neuron growth rate and terminal number by constructing a uniform-stress-distributed environment. Inspired by the three-dimensional (3D) microenvironment where cerebrospinal-fluid-contacting neurons are located, the surface curvature of the traditional rectangular-section microfluidic channel (RMC) was adjusted to construct structures with 3D curved surfaces. Compared with those on the RMC chips, the average growth rate of the axons on the AMC chips increased by 8.9% within 19 days, and the average number of terminals increased by 14.9%. This platform provides a structure that can effectively promote neuron growth and has potential in constructing more complex functional neural interfaces.

INTRODUCTION

Promoting axonal growth performance, especially increasing axon growth rate and the number of terminal branches, helps to efficiently construct neural interfaces with complex pathways.[1–4] Microfluidic chips can provide a microscale dynamic and complex biomimetic mechanical environment for increasing the axonal growth performance, serving as a typical platform for constructing neural interfaces. It provides unique advantages, including precise fluid manipulation,[5–7] high customizability,[8–11] and high spatial and temporal resolution.[12–18] Therefore, microfluidic chips can integrate microstructures sized for neurons and combine them with biological factors to investigate the effects of fluids on the axonal growth performance. In addition, the velocity and direction of the fluid in the microfluidic channel (MC) can be precisely controlled by constructing a pressure gradient to study the discrete directed growth of neurons.[19–21] By inducing discrete directed growth of neurons in a fluidic environment, microfluidic chips can provide neural interfaces with ordered networks and have great potential in neural connectivity and signal transduction.

Most of the existing microfluidic chips that induce discrete directed growth of neurons adopt the classic "Campenot" design[22] and the "Taylor platform." [23] Fluid separation between compartments enables independent drug testing on the soma or axons. MCs with ultrahigh aspect ratios isolate the soma and the axons. ensuring directed axonal growth and preventing soma invasion.[24–26] Soft lithography is widely used in the fabrication of these ultrahigh aspect ratio MCs due to its high precision, low cost, and mass production. Park et al. fabricated an MC array based on micro-macro hybrid soft-lithography master (MMHSM) fabrication technique to form a microfluidic device with a multi-chamber neuron coculture platform.[27] Dupuit et al. employed soft lithography to construct a microfluidic circuit, facilitating enhanced growth and selection of neurons at the sensing site.[28] However, the MCs in these studies were mostly rectangular-section microfluidic channels (RMCs) with sharp 90° nonbiological edges owing to limitations in the fabrication process. This makes it challenging to accurately replicate real organ morphology and fluid environments *in vivo*. The mismatched growth environment may lead to the subdifferentiation of axons, limiting the growth performance and developmental potential of neurons. Studies have indicated that axon growth in fluid dynamic cultures is affected by the internal structure of the MCs.[26,29,30] Therefore, an MC that more accurately simulates the natural *in vivo* environments where neurons develop needs to be constructed to enhance axonal extension and interactions between the neurons and their surrounding environment.

In the human body, organs or structures with ultrahigh aspect ratios involved in fluid transport, such as blood vessels, renal tubules, and the cerebral aqueduct, all have smooth inner walls. This smooth inner wall adheres to biomechanical principles and enhances the uniform

[1]Intelligent Robotics Institute, School of Mechatronical Engineering, Beijing Institute of Technology, Beijing 100081, China
[2]Laboratory for Translational Engineering, Harvard Medical School, Cambridge, MA 02139, USA
[3]Peking University First Hospital, Xicheng District, Beijing 100034, China
[4]Beijing Advanced Innovation Center for Intelligent Robots and Systems, Beijing Institute of Technology, Beijing 100081, China
[5]Key Laboratory of Biomimetic Robots and Systems (Beijing Institute of Technology), Ministry of Education, Beijing 100081, China
[6]Lead contact
*Correspondence: wanghuaping@bit.edu.cn
https://doi.org/10.1016/j.isci.2024.110885

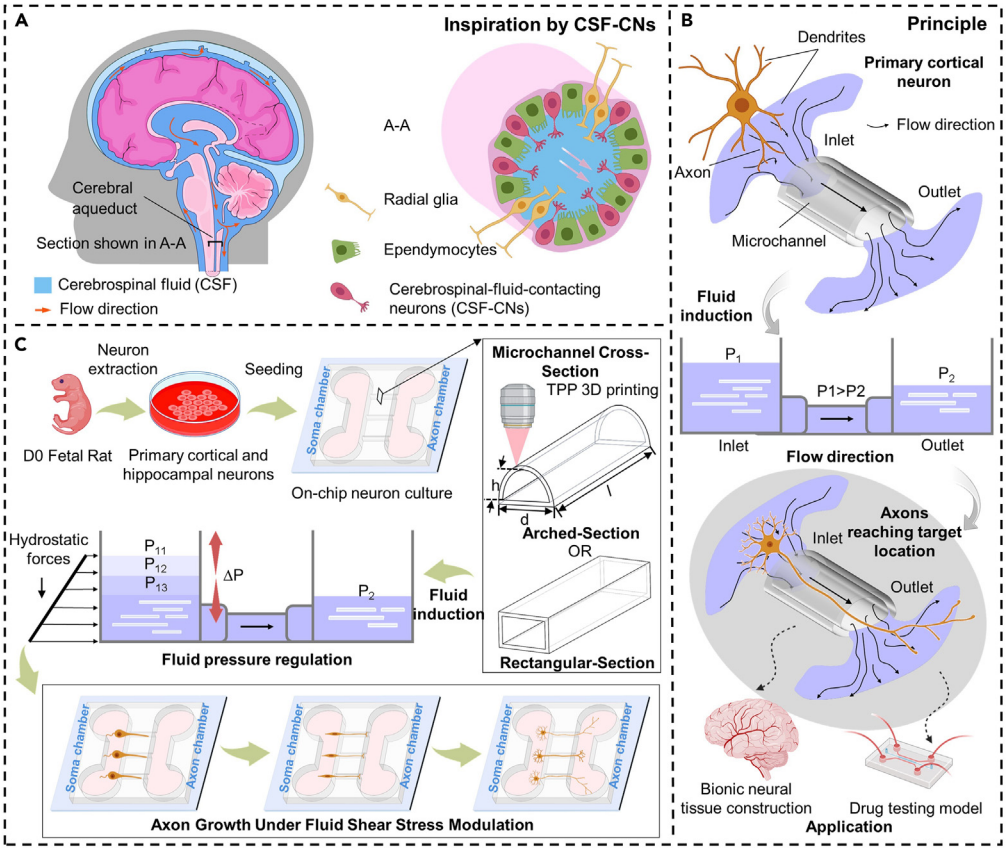

Figure 1. Conceptual overview of the AMC chips inducing discrete and directed growth of neurons based on AMCs inspired by the cerebral aqueduct

(A) Schematic of the cerebral aqueduct and its cross-section.

(B) Driving principle of the hydrostatic pressure in the AMCs for the discrete directed growth of primary cortical neurons (PCNs).

(C) Experimental process of the discrete directed growth of the PCNs in the AMCs under fluid pressure regulation.

distribution of internal shear stress; this is vitally important for preserving the structural integrity and functional stability of hollow organs.[31–34] Continuous uniform shear stress can promote changes in cell morphology and contribute to the formation of growth cones and the directional development of synapses.[35–37] In particular, the cerebral aqueduct not only serves as a crucial functional unit for circulating cerebrospinal fluid but also provides a special fluid environment for the growth of an important type of neuron in the brain—cerebrospinal-fluid-contacting neurons.[38,39] Therefore, this biophilic structure with a smooth inner wall has great potential for studies on fluid-induced directed growth of neurons. With the development of advanced fabrication technology, the use of biophilic morphology in MC patterning has increased. He et al. fabricated multilayered arched microchannels with locally smooth inner walls using a sacrificial printing method to culture ovarian cancer cells. However, the minimum diameter of the MCs could only reach 40 μm limited by the air pressure and heating temperature.[40] Qiu et al. effectively improved the printing accuracy of semicircular open MCs based on digital light processing (DLP) technology. However, constructing micron-scale arched-section microfluidic channels (AMCs) remains challenging due to manufacturing limitations.[41] Moreover, since independent axon experiments require centimeter-scale chambers and micrometer-scale MCs, manufacturing microfluidic chips that combine cross-scale capabilities with high precision is significantly challenging. Although split design and manufacturing can effectively meet the challenges of cross-scale manufacturing, they also cause difficulties in high-precision alignment and connection steps. Therefore, a high-precision, cross-scale microfluidic chip with biophilic MCs urgently needs to be developed to promote axonal growth performance.

In this study, we designed and fabricated a microfluidic chip with AMCs to form a uniform-stress-distributed microenvironment that promoted the growth performance of rat primary cortical neurons (PCNs), as shown in the schematic in Figures 1A–1C. To establish a uniform-stress-distributed environment at the microscale, we optimized the design of AMC and analyzed the distribution characteristics of the internal shear stress within AMCs by varying the fillet radii. The optimized AMCs were fabricated by two-photon polymerization (TPP). To accurately assess the impact of the MC structures on the axonal growth rate and terminal number, we measured the surface morphology of the fabricated AMCs using a digital holographic microscope (DHM) system and compared their morphologies to those of the RMCs. PCNs in the AMC chips induced by pressure differences showed significant differentiation characteristics during long-term culture. Dynamic perfusion culture of neurons was conducted in the RMC chips and AMC chips to verify the optimization of axonal growth performance in a uniform-stress-distributed microenvironment. The experimental results showed that AMCs could promote axonal growth better than RMCs under the

same pressure. Furthermore, the response of the axonal growth performance within the AMCs to different pressures was investigated. The axonal growth rate within the experimental pressure range increased as the pressure difference increased. The proposed structure can be used to construct the microenvironment with uniform fluidic stress distribution to enhance the axonal growth rate and terminal number and shows promise to develop more efficient and complex neural interfaces for neural connection and signal conduction.

RESULTS

Numerical analysis of the AMC

The internal structure of MCs can influence the distribution of fluid shear stress, which in turn regulates cellular behavior within the MCs.[42–44] To obtain an MC structure with a uniform internal shear stress distribution, a numerical model of the MC was established. The MC proposed in this study is simplified into a horizontally placed micropipe flow model, and the relationship between the flow rate and the pressure difference at both ends of the MC is described based on the generalized Hagen-Poiseuille equation[45]:

$$v = \frac{R^2 \Delta P}{8 \mu l} \quad \text{(Equation 1)}$$

where v is the fluid velocity, l is the length of the MC, R is the hydraulic radius of the MC, the ratio of the water cross-sectional area to the wetted circumference is the hydraulic radius, ΔP is the pressure difference at both ends of the MC, and μ is the dynamic viscosity of the fluid.

The shear stress in an MC is generated by the relative motion between parts of the fluid during laminar flow, and its relationship to the pressure difference at both ends of the MC can be described as follows:

$$\tau_s = \mu \frac{\partial v}{\partial r} = -\frac{\Delta P}{2l} r \quad \text{(Equation 2)}$$

where r is the radial distance from the center of the MC.

To further analyze the impact of the internal structure of the MC on the fluid environment, the shear stress distribution was simulated in the MC with different internal structures. The two vertex corners of the RMC cross-section were rounded. MCs with different internal structures were constructed by setting different round radii, as shown in Figure 2A. Considering the changes in the neuron size before and after differentiation and the possibility of the soma blocking the MC, the width and maximum height of the MC were set to 6 μm and 3 μm, respectively. When the fillet radius R_1 was set to 0, 1, 2, and 3 μm, the cross-sectional shapes of the MC changed from rectangle to arch 1, arch 2, and semicircle, corresponding to the RMC, arch 1 microfluidic channel (A1MC), arch 2 microfluidic channel (A2MC), and AMC, respectively, as illustrated in Figure 2B. The cross-section of the MC inlet (x = 0) was used to compare the size and distribution of the local shear stress across the four types of MCs. Mesh partitioning was performed on MCs with four different cross-sections to ensure that the mesh was sufficiently refined to capture the details of fluid dynamics. One end of the MC was set as the inlet with an initial pressure value of 5.5 Pa, and the outlet was set to zero pressure. The shear stress field distributions in the inlet sections of the four MCs are shown in Figures 2C–2F. The shear stress within the MCs gradually increased from the edges toward the center. To compare the distribution of shear stress more clearly in the MCs, 75 points were randomly selected from the simulation results of each MC, and the shear stresses at these points were recorded. By plotting the shear stress at random points in the coordinate system as scatter points, the shape and range of the shear stress distribution could be observed, as shown in Figures 2G–2J. The trendlines of the shear stress in the four MCs were derived by fitting the data points using a quadratic regression analysis method, as shown in Figure 2K. Under this initial pressure, the maximum shear stress within the MC decreased as R_1 increased. The mean, median, extremum, and interquartile range of the shear stress of the four MCs were calculated, and their uniformity was compared (Figure 2L). Compared with those of the other MCs, the maximum value, average value, and range of shear stress in the AMC were the lowest. The interquartile range (IQR) reflects the dispersion of the middle 50% of the data. A larger IQR indicates greater dispersion in the middle portion of the data; a smaller IQR indicates more concentrated data. Therefore, under the same pressure, the shear stress distribution within the AMC was relatively uniform. Based on the simulation results, compared to the other three MCs, the AMC effectively promoted a uniform distribution of shear stress and reduced the local stress peaks. Therefore, in this study, AMC chips were selected as the main platform for the directed growth of neurons and compared with the classic RMC chips.

Characterization of the AMC

The morphology of the MC directly affects the shear stress distribution of the internal fluid environment. Therefore, the high-precision preparation of MCs with bionic morphology is crucial for constructing a uniform-stress-distributed environment *in vitro*. To more accurately assess the impact of MC structures on axonal growth rates, the inner surface morphology of the prepared AMCs and RMCs was characterized based on the DHM system. Three-dimensional (3D) holographic images of the RMCs and AMCs are shown in Figures 3A and 3B. Through the enlarged cross-section of a single MC, clear rectangular and arched outlines could be observed. Four sections, A, B, C, and D, were randomly taken perpendicular to the MC, and the inner surface profiles of the RMCs and AMCs on the four sections were measured, as shown in Figures 3C and 3D. After assembling the AMC chip, Rhodamine 6G dye was infused from the soma chamber until it filled the entire chip cavity to further characterize the encapsulated AMC structure (Figure S1). These results showed that TPP-based RMCs and AMCs had target surfaces, which could provide conditions for precise control of the shear stress distribution of the internal fluid environment.

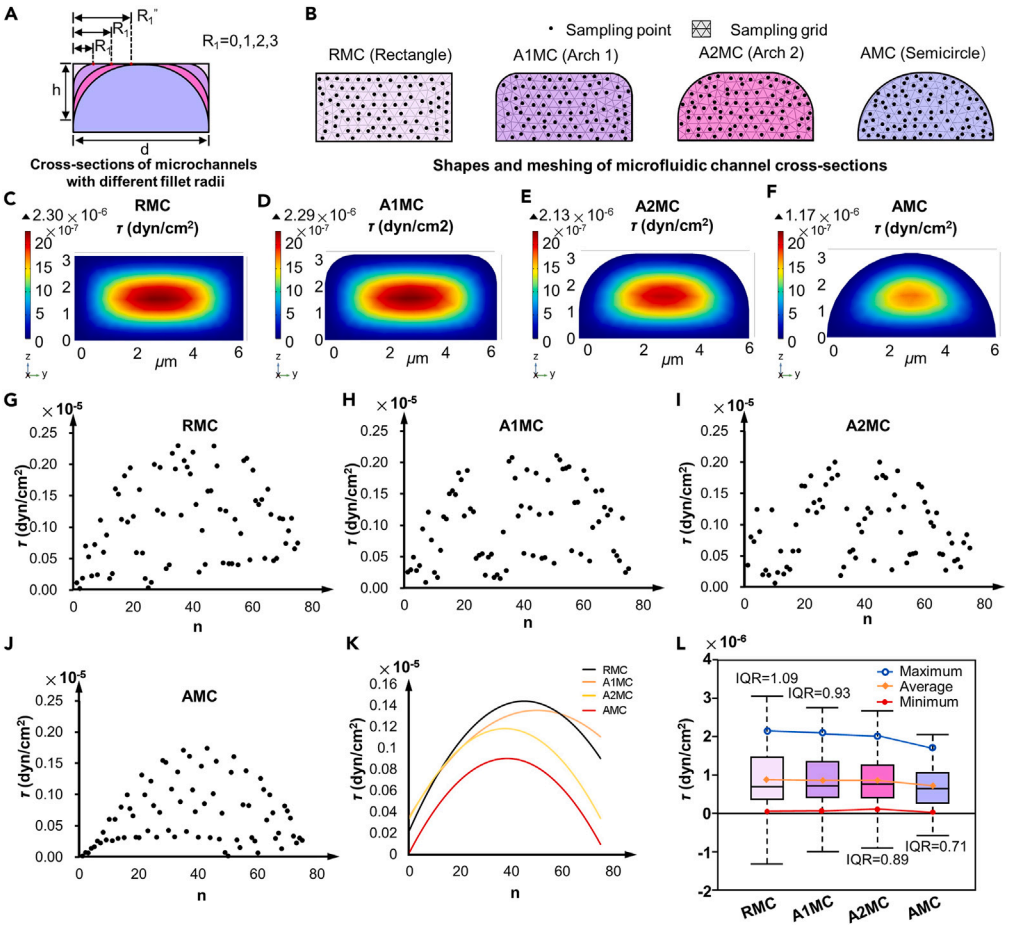

Figure 2. Simulation results of the shear stress distribution in MCs with four different fillet radii

(A) Fillet radii values for the cross-sections of the four types of MCs.

(B) Shapes and meshing of the MC cross-sections.

(C–F) Shear stress field distribution in the four types of MCs under the same pressure.

(G–J) Scatterplots of the shear stress distribution in the four types of MCs.

(K) Trendlines of the shear stress in the four types of MCs.

(L) Comparison of the shear stress uniformity within the four MCs, including the maximum, average, and minimum values.

Promotion of axonal differentiation within AMCs

Shear stress within MCs can influence axonal growth through physical stimulation.[29] To understand the effect of the MC structure on axonal growth, the axonal growth rate and length of PCNs in AMCs and RMCs were monitored every day under the same conditions (Figures 4A–4C). Here, the average length of the axons represents the effective length, which is defined as the distance from the MC outlet to the axon terminal along the direction of the MC. For comparison, the slides in petri dishes were also used to culture PCNs under the same conditions. During the 4-day culture process, the neurons growing on the slides were not affected by directional flow, and their axons spread throughout the entire slide and overlapped in a disorderly manner (Figure 4D). In contrast, neurons in the soma chamber differentiated to form axons (green) that entered and extended along the MC to reach the axon chamber, as shown in Figures 4E and 4F. The red dotted line marks the outlet location of the MCs. Notably, on day 4, the axons in the AMCs had already extended approximately 50 μm beyond the MC outlet, whereas the axons in the RMCs had just begun to reach the MC outlet. The average times for the axons in AMCs and RMCs to reach the outlets are shown in Figure 4G. The neuronal axons in the AMCs group exhibited a higher growth rate than those in the RMCs group (Figure 4H). On day 2, the average growth rate of axons in the AMC group reached 57 μm/day; this was an increase of 27.9% compared to that in the RMC group. Consequently, the axon length within the AMCs was consistently greater than that within the RMCs (Figure 4I). Due to the directional and regional restrictions placed on the axonal growth, the growth rates of axons in both AMCs and RMCs were lower than those induced by nondirectional fluid flow. Based on these results, compared to traditional RMCs, AMCs could effectively enhance the growth rate of the PCN axons within the MCs. In summary, AMCs effectively promoted the growth of PCN axons inside MCs. By providing a more suitable fluidic environment for axonal growth, AMCs potentially play a role in maintaining and enhancing the directed growth of PCN axons in a confined environment.

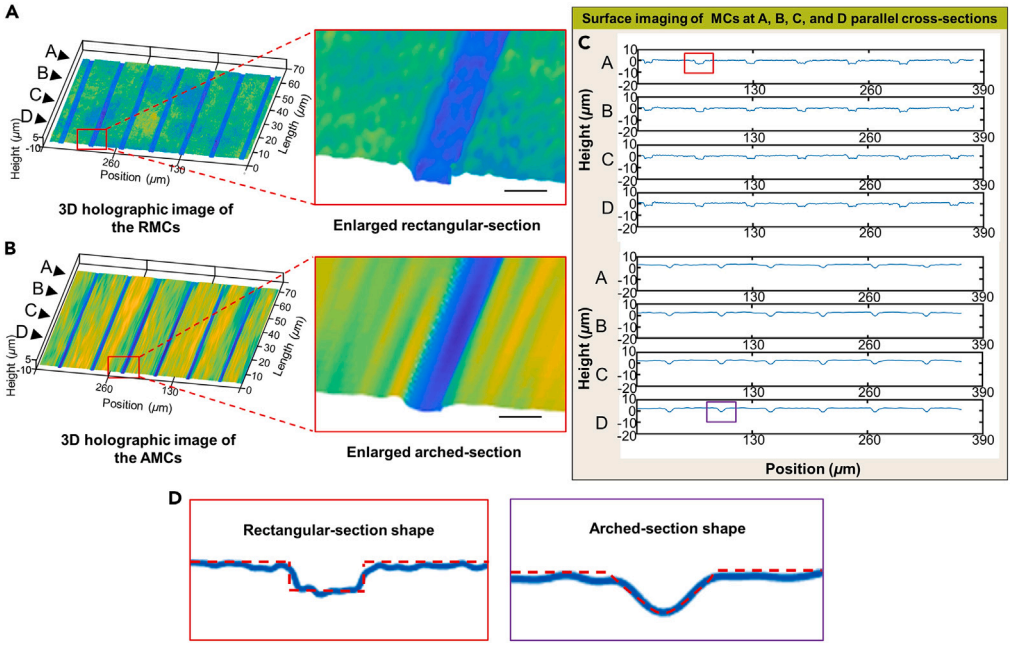

Figure 3. Holographic phase reconstruction images of AMCs and RMCs under a digital holographic microscope (DHM system)

(A) 3D holographic image and enlarged image of the AMCs.

(B) 3D holographic image and enlarged image of the RMCs.

(C) Cross-sections of the AMCs and RMCs in planes A, B, C, and D. Planes A, B, C, and D are parallel to the cross-sections of the MCs.

(D) The enlarged shapes of the cross-sections. The red dashed line represents the surface contour. Scale bar: 6 μm.

Promotion of axonal differentiation beyond AMCs

To further understand the impact of the MC structure on axonal growth outside the MCs, the growth rates, and lengths of PCN axons growing out of AMCs and RMCs were monitored daily under the same conditions, as shown in Figure 5. Assuming that the axons reached the MC outlet on day D_0, the growth performance of the axons in the AMC and RMC groups was compared on days D_0+1, D_0+4, and D_0+7 after they grew out of the MCs. Over a 7-day continuous culture period, the axons in both the AMC and RMC groups (green) continued to grow along the extension direction of the MC length, gradually dispersing as the number of culture days increased, as illustrated in Figures 5A–5F. However, the axons outside the AMCs exhibited greater growth than those outside the RMCs from day D_0+1 through day D_0+7, as shown in Figure 5G. Notably, the axon growth rate gradually decreased from day D_0+1 to day D_0+3 but significantly increased on day D_0+4, likely due to the introduction of the fresh differentiation medium providing new growth factors and nutrients. After an extended culture period, the axon length outside the AMCs remained greater than that outside the RMCs (Figure 5H). On day D_0+7, the axon length outside the AMCs was 13.2% longer than that outside the RMCs. Based on the immunofluorescence staining results, compared to the traditional RMCs, the enhanced uniform stress environment within the AMC still promoted and guided the extension of axons outside the MCs.

In *in vitro* neural models, the number of axonal terminals significantly influences the structure and function of neuronal networks. To further investigate this influence, we monitored the number of axonal terminals in the AMC and RMC groups from day D_0+1 to day D_0+7. Ten MCs were randomly selected for sampling, and the number of axonal terminals within these MCs was quantified. Each distal tip of an axon was considered an axonal terminal, with each axon possessing multiple terminals. Throughout the culture period, the average number of axonal terminals in the AMC group consistently exceeded that in the RMC group, as illustrated in Figure 5I. On day D_0+7, the average number of axonal terminals in the AMC group reached its peak, showing a 7.2% increase compared to that in the RMC group. Overall, these findings indicate that AMCs could play a role in maintaining and promoting the directional growth of PCN axons, even with only physical constraints on local neuronal axons.

To assess the ultimate effects of cultivating neurons in the AMC chips and RMC chips, the neurons were continuously cultured in both types of MCs until day 19, when axonal terminals reached the right edge of the MCs. Due to axonal retraction or breakage observed after day 19, this day was selected as the final day of culture. The axon performance of the AMC chips and RMC chips on day 19 is compared in Figure 6. Global fluorescence images of the axons within the AMC chips and RMC chips on day 19 after treatment with GFAP (red), βIII tubulin (green), and Hoechst 33258 (blue) are shown in Figures 6A and 6B. By zooming into the axonal terminal areas, on day 19, some axonal terminals in both the AMC chips and RMC chips reached the furthest edge of the axon chamber (Figures 6C and 6D). Even 7 days after the axons grew out of the MCs, the average axon length and average number of terminals in the AMC chip group were still greater than those in the RMC chip group. The average axon length and number of axon terminals per 10 channels within the AMC chips and RMC chips on day 19 are shown in

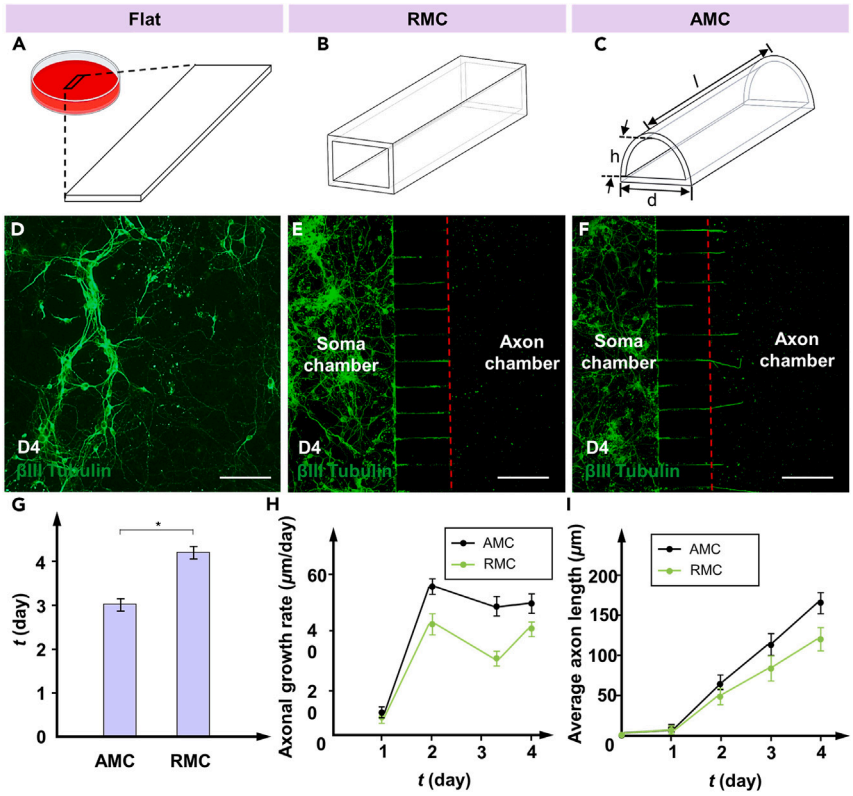

Figure 4. Axonal growth rates within MCs and the control group

(A–C) Flat, RMC, and AMC for neuron culture.

(D–F) Images of the axon growth within the flat, RMC, and AMC groups after βIII-tubulin treatment. The axon extends from the left soma chamber to the axon chamber under the induction of shear stress. The red dotted line marks the outlet location of the MCs.

(G) Average time for the axons in AMCs and RMCs to reach the outlets.

(H) Average axonal growth rate within different MCs.

(I) Average axon length within different MCs. The data are presented as the mean ± standard deviation (n = 3). *p < 0.05. Scale bar: 120 μm.

Figures 6E and 6F. Notably, on the last day of the cell culture, soma invasion in the RMC chip group was evident. The number of cells (including neurons [green] and astrocytes [red]) that invaded the axon chamber in the AMC chips and RMC chips was evaluated per 10 MCs throughout the long-term culture process, as shown in Figure 6G. As the number of culture days increased, the number of neurons invading the axon chamber in the RMC chip group gradually increased, reaching an average of 5.6 neurons per 10 channels on day 19. In contrast, soma invasion in the AMC chip group was extremely rare, with only an average of 2 neurons leaking out of every 10 MCs on day 19. The effective isolation of the neuron somas and axons by the AMC chips helps to construct independent axonal physical units and improves the accuracy of drug testing in axonal injury experiments. In summary, these results indicate that during long-term dynamic culture, even 7 days after axons have grown out of the MCs, the axons within the AMC chips are able to maintain a high growth rate and steady terminal number. Additionally, they effectively reduce the incidence of invasion of the axon chambers by the neuronal soma.

Promotion of axonal differentiation under enhanced pressure

Pressure can influence the behavior and direction of growth cones by affecting the interactions between the cytoskeleton and the extracellular matrix.[26,46] To further explore the effect of changes in pressure on the axonal growth, neuronal differentiation experiments with AMC chips were conducted under three pressures. Different pressures within the chip are achieved by increasing and decreasing the fluid volume difference between the two chambers. Among them, the medium pressure ΔP_m is the same as the previous pressure to compare the changes in the axonal behavior under higher (ΔP_h = 7.5 Pa) and lower pressures (ΔP_l = 3.5 Pa). Since excessively high pressure gradient can cause cells to block the MC entrance, and excessively low pressure gradient cannot induce axons to enter the MC, the pressure gradient of 5.5 Pa used in similar studies was determined to be a compromise for the appropriate culture environment.[20] Considering the maximum and minimum volumes of the liquid reservoir, higher and lower pressure gradients of 3.5 Pa and 7.5 Pa were selected as comparison groups for the experiment. Figure 7A shows AMC chips under pressure with ΔP_h, ΔP_m, and ΔP_l. Fluorescence images of the axons within the AMC chips on day 19 under pressure with ΔP_h, ΔP_m, and ΔP_l after MAP-2 (green) and βIII tubulin (red) treatment are shown in Figures 7B–7D. During the culture period

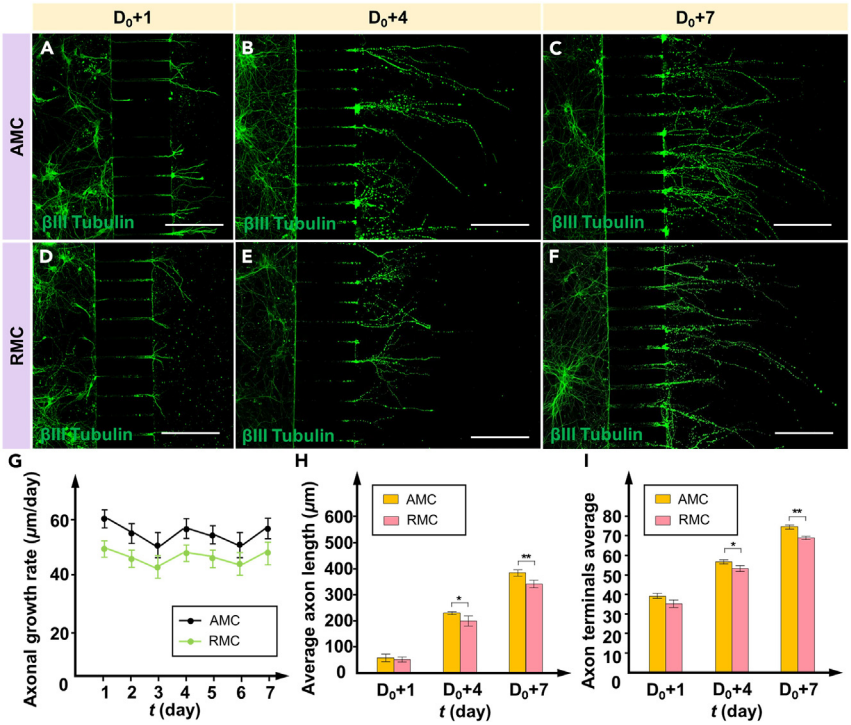

Figure 5. Axonal growth rates after extending beyond the outlet of the MCs

(A–C) Images of the axon growth outside the AMCs on days D_0+1, D_0+4, and D_0+7 after βIII tubulin treatment.

(D–F) Images of the axon growth outside the RMCs on days D_0+1, D_0+4, and D_0+7 after βIII tubulin treatment.

(G) Average axonal growth rate of the different MCs.

(H) Average axon length outside the AMCs and RMCs on days D_0+1, D_0+4, and D_0+7. Here, the average length of the axons represents the effective length, which is defined as the distance from the MC outlet to the axon terminal along the direction of the MC.

(I) Average number of axon terminals outside the AMCs and RMCs on days D_0+1, D_0+4, and D_0+7. Ten MCs were randomly selected for sampling, and the total number of axonal terminals within these MCs was quantified. Each distal tip of an axon is considered an axon terminal. Each axon has more than one terminal. The data are presented as the mean ± standard deviation (n = 3). *p < 0.05, **p < 0.01. Scale bar: 180 μm.

inside the AMCs, as the pressure increased, the average time for the axons within the AMCs to reach the outlets gradually decreased, as shown in Figure 7E. When the initial pressure was ΔP_h, the average time for the axons within the AMCs to reach the outlets could be reduced to 2.8 days; this was a decrease of 9.6% with respect to the ΔP_m group and a decrease of 16.2% with respect to the ΔP_l group. Moreover, the effects of pressure on axons persisted outside AMCs. The growth rates of the axons outside the AMCs on days D_0+1, D_0+7, and 19 under pressure with ΔP_l, ΔP_m, and ΔP_h are shown in Figure 7F. The axon growth rates on days D_0+1, D_0+7, and 19 in the ΔP_h group were always greater than those in the other two groups. The axon growth rate on day 19 reached 62 μm/day; this was an increase of 10.7% compared to that of the ΔP_l group. Furthermore, as the number of culture days increased, the axon growth rates of all groups continued to increase. The lowest axonal growth rate occurred on day 19 in the ΔP_l group, with a size of 36 μm/day; this value was 17.9% lower than that in the ΔP_h group during the same period. In addition, we compared the average axon length and average number of axon terminals per 10 MCs within the AMC chips on days D_0+1, D_0+7, and 19 under pressures of ΔP_l, ΔP_m, and ΔP_h, as shown in Figure 7G. During the culture process outside AMCs, compared with that in the ΔP_m group, the axon length in the ΔP_l group was significantly reduced and reached a maximum difference of approximately 330 μm on day D_0+7. At the same time, the number of axon terminals in the ΔP_l group was always smaller than that in the ΔP_m group. Notably, as the pressure increased, the axon growth length and the number of axon terminals in the ΔP_h group only slightly increased compared with those in the ΔP_m group; this result was different from the significant increase in the ΔP_m group compared with the ΔP_l group. In summary, these results demonstrate that within the range of pressures used in the experiments, increasing the pressure can promote axonal growth and effectively increase the number of axonal terminals. However, as the pressure continues to increase, its stimulatory effect on axonal growth weakens.

Effects of the MC structure and pressure on the axon orientation

Axon orientation has a significant impact on the organization and function of neural networks. Concentrated axonal alignment facilitates the construction of highly organized neuronal networks, significantly enhancing the speed and efficiency of signal transmission. Therefore, we further explored the effects of the MC structures and pressure on the axon orientation. The axon orientations in the RMC chips under

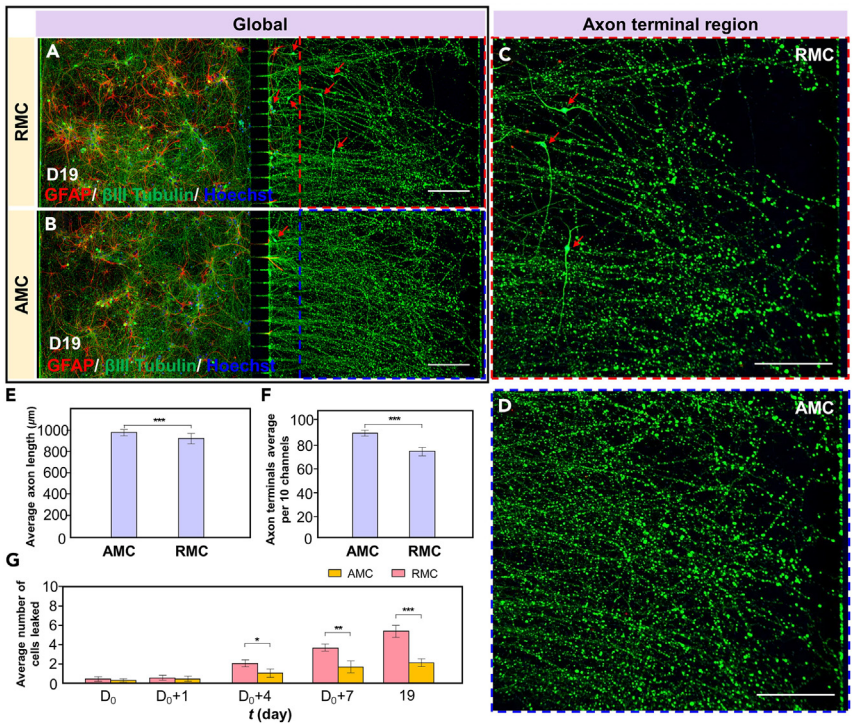

Figure 6. Axon growth within the AMC chips and RMC chips on day 19

(A and B) Fluorescence images of axons within the microfluidic chips with AMCs and RMCs on day 19 after GFAP (red), βIII tubulin (green), and Hoechst 33258 (blue) treatment.

(C and D) Enlarged images of the axon terminal regions within the AMC chips and RMC chips.

(E) Average axon length within the AMC chips and RMC chips on day 19.

(F) Average number of axon terminals per 10 MCs within the AMC chips and RMC chips on day 19.

(G) Average number of cells that leaked per 10 MCs within AMC chips and RMC chips on days D_0+1, D_0+4, D_0+7, and 19. The data are presented as the mean ± standard deviation (n = 3). *p < 0.05, **p < 0.01, ***p < 0.001. Scale bar: 130 μm.

ΔP_m, AMC chips under ΔP_m, and AMC chips under ΔP_h were measured and counted, as shown in Figure 8. Figure 8A shows a schematic diagram of the direction and angle of axon growth. To describe and compare the distribution of axon angles more clearly, rose diagrams were used to determine axon orientation. A rose diagram representing the corresponding angle range was constructed for every 12 sectors. The size of the sector radius represents the number of axons within this angle range. For comparison, the axon orientation of the neurons on slides in petri dishes was measured as the control group, as shown in Figure 8B. A comparison of the growth angles of the axons in the RMC chips and AMC chips revealed that the axon orientation of the AMC group showed a significant centralized orientation trend after a long-term dynamic culture, indicating that the shear-stress-induced axon orientation was related to the structure of the MC (Figures 8C and 8D). To assess the degree of axonal alignment along the direction of the MCs, the percentage of axons oriented at angles between 75° and 115° within the RMC chips, AMC chips, and AMC chips under high pressure (ΔP_h) was calculated, as shown in Figure 8F. The results showed that the number of axons oriented in the range of 75°–115° in the AMC group was significantly greater than that in the RMC group, and this difference became more significant with increasing pressure.

Based on these experiments, compared to the RMC chips, the AMC chips can more effectively increase the concentration of the axons in the target direction; this result is consistent with the results from the fluid simulation analysis. This potentially occurs because the smooth surface inside the AMC reduces the fluid resistance generated when the fluid flows, thereby reducing mechanical interference on axons. In addition, an increase in the pressure applied across both ends of the AMC can promote the further concentration of the axon direction along the direction of the pressure. This finding is consistent with previous findings showing that high shear stress can induce cell reorientation.[47]

DISCUSSION

MCs in microfluidic chips can facilitate neuronal growth, playing a key role in developing neural interfaces with ordered pathways. Some studies have developed axon tractors or 3D guiding conduits as models to enhance the growth rate of neurons.[48–50] In these studies, researchers stimulated axonal growth using axon pullers like PDMS barriers or growth substrates such as collagen. However, axonal growth performance is inextricably linked to the natural 3D environment and fluid stimulation.[51] In this study, we designed and fabricated an AMC chip to increase axonal growth rate and terminal number. We used TPP and soft lithography techniques to create an AMC chip with

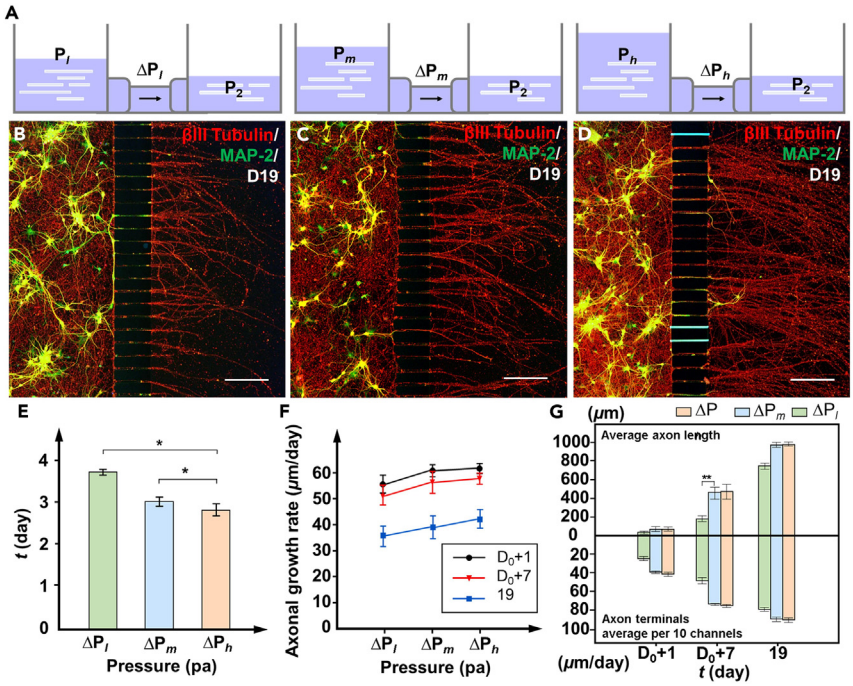

Figure 7. Axonal growth within AMC chips under different pressures

(A) AMC chips under pressure with ΔP_l, ΔP_m, and ΔP_h.

(B–D) Fluorescence images of axons within the AMC chips on day 19 under pressure with ΔP_l, ΔP_m, and ΔP_h after MAP-2 (green) and βIII tubulin (red) treatment.

(E) Average time for the axons within the AMCs under pressure with ΔP_l, ΔP_m, and ΔP_h to reach the outlets.

(F) Axonal growth rate outside the AMCs on days D_0+1, D_0+7, and 19 under pressure with ΔP_l, ΔP_m, and ΔP_h.

(G) Average axon length and average number of axon terminals per 10 MCs within the AMC chips on days D_0+1, D_0+7, and 19 under pressure with ΔP_l, ΔP_m, and ΔP_h. The data are presented as the mean ± standard deviation (n = 3). *p < 0.05, **p < 0.01. Scale bar: 230 μm.

a 3D structure to construct a fluid environment for neuronal growth. Compared to traditional neuro-microfluidic systems,[22,23,25] our AMC chip offers the combined advantages of cross-scale capability, high precision, high efficiency, and maskless fabrication.

Inspired by the environment where neurons are in contact with cerebrospinal fluid, the AMC microstructure has a gentle top surface that provides uniformly distributed shear stress, creating conditions to enhance axonal growth performance. Neuron culture results indicated that the AMC structure positively affect the growth and maintenance of PCN axons within MCs. This effect shows the high sensitivity of axonal performance to the enclosed microenvironment structure and the resulting shear stress, which is consistent with conclusions from previous studies.[29] In this related research, cells in MCs with an arched cross-section had stronger adhesion compared to those in MCs with a square cross-section, providing more possibilities for changing shape in response to mechanical stimuli.

After the axons grow out of the MCs, the front part of the axons is still affected by the fluid environment within the MCs. Axons beyond the AMC showed a greater growth rate than axons beyond the RMC, and the overall growth rate was higher than that inside the MC. The reason for this difference is the axonal terminals outside the MCs are in a non-enclosed environment that offers more nutrients and fewer physical constraints. The number of axon terminals is a key factor affecting the structure and function of neuronal networks. The average number of axon terminals outside the MC in the AMC group was continuously higher than that in the RMC group. Furthermore, the average number of axonal terminals increased with culture time. This result aligned with our expectations, as accumulated nutrients like nerve growth factors during cultivation promote axonal branching.

Except for the MC structure, pressure can influence the migration and positioning of neurons by altering the mechanical environment. Within AMCs, the axonal growth rate increased with pressure, and this phenomenon continued beyond AMCs. It was consistent with published studies of axonal responses to mechanical stimulation.[52] The results indicated that pressure positively influenced the increase in axon terminals within the experimental range. This likely resulted from pressure-induced mechanical stimulation activating mechanosensitive ion channels or altering gene expression. The interesting mechanism behind this is worth exploring further.

The potential mechanisms by which fluid shear stress affects PCN axon morphology require further investigation. The process by which neurons develop and extend their axons from the cell body is driven by the cytoskeleton.[53] Cytoskeletal dynamics are the foundation of axonal growth, determining the direction and rate of elongation. Specifically, actin filaments regulate the shape and directed growth of the growth cone, whereas microtubules provide the axonal shaft structure, which is crucial for axonal extension.[54] Fluid shear stress acts as a mechanical stimulus that can affect actin and microtubules, leading to changes in cell morphology.[55] In addition to the cytoskeleton, cellular

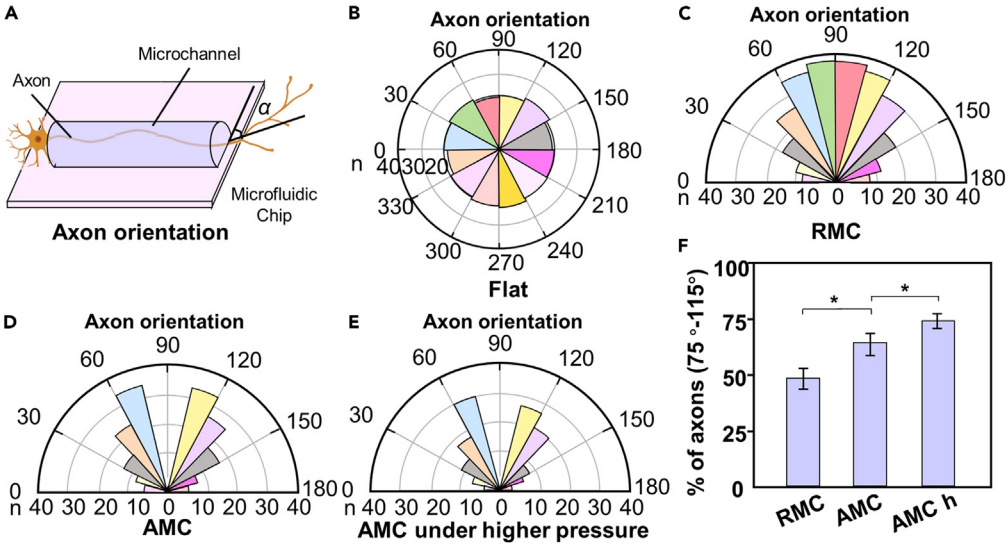

Figure 8. Axon orientation within different MCs and under different pressures

(A) Schematic diagram of the direction and angle of axon growth.

(B) Axonal orientation of the neurons on slides in petri dishes (control group). The size of the sector radius represents the number of axons within this angle range.

(C and D) Axonal orientation of the average number of neurons per 10 MCs within the RMC chips and AMC chips.

(E) Axonal orientation of the neurons within the AMC chips under ΔP_h.

(F) Percentage of axons oriented at 75°–115° within the RMC chips, AMC chips, and AMC chips under ΔP_h. The data are presented as the mean ± standard deviation ($n = 3$). *$p < 0.05$.

mechanoreceptors such as β1 integrins, focal adhesions, and mechanosensitive ion channels also play a role in how cells sense and respond to mechanical environments. Fluid shear stress regulates intracellular signaling pathways (such as Rho GTPase, PI3K/Akt, and MAPK), specific genes (such as ALP, OCN, Runx2, and COLI α), and proteins (such as FLK-1, ERK1/2, etc.) by activating these mechanoreceptors, thereby influencing cell morphology.[56–59] For example, in human mesenchymal stem cells, fluid shear stress can activate ERK1/2, which in turn activates Runx2 to promote osteogenic differentiation and morphological changes in the cells. Several studies have shown that fluid shear stress can trigger a series of complex coupled molecular biological responses, thereby promoting changes in cortical neuron morphology.[20,23,26] Nevertheless, there is still limited research on how axons sense fluid shear stress and transmit these signals internally within neurons to induce changes in axonal morphology.

Based on the findings of this study regarding the effects of microfluidic chip structure and pressure on neuronal morphology, we can further refine the regulatory strategies for neuronal morphology. Considering the complex growth environment of neurons, the growth of neurons is affected by complex interactions among factors such as growth factors, the extracellular matrix, and mechanical force. In future work, the study of the regulatory mechanism of this complex interaction will be the main research direction. Furthermore, how to regulate neuronal growth based on these complex interactions to construct complex functional neural interfaces is also a major issue we aim to address. The evaluation of the axonal growth in this study demonstrated the feasibility of our method for establishing a valuable *in vitro* biomimetic model for regulating neural growth, which can aid in understanding the structural and functional adaptations of the nervous system to environmental changes and other factors and help develop therapeutic strategies for treating axonal injuries and degenerative diseases.

Limitations of the study

Although we have proposed the effects of MC structure and pressure gradients on PCN morphology, the specific regulatory mechanisms by which fluid dynamics influence neuronal morphology still require further exploration in our future work. Similar to endothelial cells and human mesenchymal stem cells, axons sense the stimulation of fluid shear stress and transmit it internally within neurons to trigger a series of biological effects. We believe that the activation of mechanoreceptors in cells, such as integrins, focal adhesions, and mechanosensitive ion channels, may be an intermediate process in axonal morphological changes. These complex processes of change are likely the result of the combined actions of multiple regulatory factors. Another possible mechanism is that the uniform distribution of shear stress enhances the directional aggregation and alignment of actin filaments and microtubules within the cell, thereby promoting directional cell migration and morphological remodeling. Molecular biology techniques can reveal the structure, function, and interactions of intracellular biomolecules (such as DNA, RNA, and proteins), serving as important tools for studying the specific regulatory mechanisms of axonal growth. Additionally, the brain tissue in this study was used irrespective of biological sex; it would be interesting to conduct similar assays in the future with cultures of male and female cells separately and compare the results. We still need to make further efforts to identify

potential regulatory mechanisms through additional experimental approaches, providing modest guidance for the construction of complex neural networks.

RESOURCE AVAILABILITY

Lead contact

Further information and requests for resources should be directed to and will be fulfilled by the lead contact, Huaping Wang (wanghuaping@bit.edu.cn).

Materials availability

This study did not generate new unique reagents.

Data and code availability

- All data needed to evaluate the conclusions in the paper are present in the article. The datasets generated and/or analyzed during the current study are available from the lead contact upon reasonable request.
- This paper does not report original code.
- Any additional information required to reanalyze the data reported in this paper is available from the lead contact upon request.

ACKNOWLEDGMENTS

This work was supported by National Key Research and Development Program of China under grant 2023YFB4705400; the National Natural Science Foundation of China under grant numbers 62222305, 62073042, and U22A2064; and Postdoctoral Fellowship Program of CPSF under grant BX20230459.

AUTHOR CONTRIBUTIONS

M.H.L. conceived the work. H.P.W., A.P.W., and M.H.L. performed the experiments. J.X.L. drafted the manuscript. Y.L. did the simulation. H.-W.H., Q.S., and Q.H. analyzed the data.

DECLARATION OF INTERESTS

The authors declare that they have no competing interests.

STAR★METHODS

Detailed methods are provided in the online version of this paper and include the following:

- KEY RESOURCES TABLE
- EXPERIMENTAL MODEL AND STUDY PARTICIPANT DETAILS
  - Neuron culture and maintenance
- METHOD DETAILS
  - Preparation of the microfluidic chips with AMCs
  - DHM system
  - Simulation analysis
  - Immunofluorescence staining
- QUANTIFICATION AND STATISTICAL ANALYSIS

SUPPLEMENTAL INFORMATION

Supplemental information can be found online at https://doi.org/10.1016/j.isci.2024.110885.

Received: June 20, 2024
Revised: August 2, 2024
Accepted: September 2, 2024
Published: September 4, 2024

REFERENCES

1. Acarón Ledesma, H., Li, X., Carvalho-de-Souza, J.L., Wei, W., Bezanilla, F., and Tian, B. (2019). An atlas of nano-enabled neural interfaces. Nat. Nanotechnol. *14*, 645–657.
2. Montalà-Flaquer, M., López-León, C.F., Tornero, D., Houben, A.M., Fardet, T., Monceau, P., Bottani, S., and Soriano, J. (2022). Rich dynamics and functional organization on topographically designed neuronal networks in vitro. iScience *25*, 105680.
3. Hong, J.W., Yoon, C., Jo, K., Won, J.H., and Park, S. (2021). Recent advances in recording and modulation technologies for next-generation neural interfaces. iScience *24*, 103550.
4. Stanganello, E., Zahavi, E.E., Burute, M., Smits, J., Jordens, I., Maurice, M.M., Kapitein, L.C., and Hoogenraad, C.C. (2019). Wnt signaling directs neuronal polarity and axonal growth. iScience *13*, 318–327.
5. Amartumur, S., Nguyen, H., Huynh, T., Kim, T.S., Woo, R.S., Oh, E., Kim, K.K., Lee, L.P., and Heo, C. (2024). Neuropathogenesis-on-chips for neurodegenerative diseases. Nat. Commun. *15*, 2219.
6. Zhan, Z., Liu, Z., Nan, H., Li, J., Xie, Y., and Hu, C. (2022). Heterogeneous spheroids with tunable interior morphologies by droplet-based microfluidics. Biofabrication *14*, 025024.
7. Liu, Z., Zhang, H., Zhan, Z., Nan, H., Huang, N., Xu, T., Gong, X., and Hu, C. (2021). Mild formation of core-shell hydrogel microcapsules for cell encapsulation. Biofabrication *13*, 025002.
8. Xu, X., Huang, X., Sun, J., Chen, J., Wu, G., Yao, Y., Zhou, N., Wang, S., and Sun, L. (2022). 3D-Stacked Multistage Inertial Microfluidic

Chip for High-Throughput Enrichment of Circulating Tumor Cells. Cyborg Bionic Syst. *2022*, 9829287.
9. Yin, H., Wang, Y., Liu, N., Zhong, S., Li, L., Zhang, Q., Liu, Z., and Yue, T. (2024). Advances in the Model Structure of In Vitro Vascularized Organ-on-a-Chip. Cyborg Bionic Syst. *5*, 0107.
10. Liu, Z., Nan, H., Jiang, Y., Xu, T., Gong, X., and Hu, C. (2022). Programmable Electrodeposition of Janus Alginate/Poly-L-Lysine/Alginate (APA) Microcapsules for High-Resolution Cell Patterning and Compartmentalization. Small *18*, 2106363.
11. Pan, P., Laver, J.D., Qin, Z., Zhou, Y., Peng, R., Zhao, L., Xie, H., Calarco, J.A., and Liu, X. (2021). On-chip rotation of Caenorhabditis elegans using microfluidic vortices. Adv. Mater. Technol. *6*, 2000575.
12. Yue, T., Zhao, D., Phan, D.T.T., Wang, X., Park, J.J., Biviji, Z., Hughes, C.C.W., and Lee, A.P. (2021). A modular microfluidic system based on a multilayered configuration to generate large-scale perfusable microvascular networks. Microsyst. Nanoeng. *7*, 4.
13. Sakaguchi, K., Akimoto, K., Takaira, M., Tanaka, R.I., Shimizu, T., and Umezu, S. (2022). Cell-Based Microfluidic Device Utilizing Cell Sheet Technology. Cyborg Bionic Syst. *2022*, 9758187.
14. Bai, X., Song, B., Chen, Z., Zhang, W., Chen, D., Dai, Y., Liang, S., Zhang, D., Zhao, Z., and Feng, L. (2021). Postoperative evaluation of tumours based on label-free acoustic separation of circulating tumour cells by microstreaming. Lab Chip *21*, 2721–2729.
15. Dong, X., Song, P., and Liu, X. (2019). An automated microfluidic system for morphological measurement and size-based sorting of C. elegans. IEEE Trans. NanoBioscience *18*, 373–380.
16. Hagiwara, M., Kawahara, T., and Arai, F. (2012). Local streamline generation by mechanical oscillation in a microfluidic chip for noncontact cell manipulations. Appl. Phys. Lett. *101*, 074102.
17. Chang, D., Sakuma, S., Kera, K., Uozumi, N., and Arai, F. (2018). Measurement of the mechanical properties of single Synechocystis sp. strain PCC6803 cells in different osmotic concentrations using a robot-integrated microfluidic chip. Lab Chip *18*, 1241–1249.
18. Cui, J., Wang, H.P., Shi, Q., and Sun, T. (2021). Pulsed Microfluid Force-Based On-Chip Modular Fabrication for Liver Lobule-Like 3D Cellular Models. Cyborg Bionic Syst. *2021*, 9871396.
19. Wei, Z., Sun, T., Shimoda, S., Chen, Z., Chen, X., Wang, H., Huang, Q., Fukuda, T., and Shi, Q. (2022). Bio-inspired engineering of a perfusion culture platform for guided three-dimensional nerve cell growth and differentiation. Lab Chip *22*, 1006–1017.
20. Park, J.W., Vahidi, B., Taylor, A.M., Rhee, S.W., and Jeon, N.L. (2006). Microfluidic culture platform for neuroscience research. Nat. Protoc. *1*, 2128–2136.
21. Na, S., Kang, M., Bang, S., Park, D., Kim, J., Sim, S.J., Chang, S., and Jeon, N.L. (2016). Microfluidic neural axon diode. Technology *04*, 240–248.
22. Campenot, R.B. (1977). Local control of neurite development by nerve growth factor. Proc. Natl. Acad. Sci. USA *74*, 4516–4519.
23. Taylor, A.M., Blurton-Jones, M., Rhee, S.W., Cribbs, D.H., Cotman, C.W., and Jeon, N.L. (2005). A microfluidic culture platform for CNS axonal injury, regeneration and transport. Nat. Methods *2*, 599–605.
24. Taylor, A.M., Menon, S., and Gupton, S.L. (2015). Passive microfluidic chamber for long-term imaging of axon guidance in response to soluble gradients. Lab Chip *15*, 2781–2789.
25. Jokinen, V., Sakha, P., Suvanto, P., Rivera, C., Franssila, S., Lauri, S.E., and Huttunen, H.J. (2013). A microfluidic chip for axonal isolation and electrophysiological measurements. J. Neurosci. Methods *212*, 276–282.
26. Peyrin, J.M., Deleglise, B., Saias, L., Vignes, M., Gougis, P., Magnifico, S., Betuing, S., Pietri, M., Caboche, J., Vanhoutte, P., et al. (2011). Axon diodes for the reconstruction of oriented neuronal networks in microfluidic chambers. Lab Chip *11*, 3663–3673.
27. Park, J., Li, J., and Han, A. (2010). Micro-macro hybrid soft-lithography master (MMHSM) fabrication for lab-on-a-chip applications. Biomed. Microdevices *12*, 345–351.
28. Dupuit, V., Terral, O., Bres, G., Claudel, A., Fernandez, B., Briançon-Marjollet, A., and Delacour, C. (2022). A multifunctional hybrid graphene and microfluidic platform to interface topological neuron networks. Adv. Funct. Mater. *32*, 2207001.
29. Esch, M.B., Post, D.J., Shuler, M.L., and Stokol, T. (2011). Characterization of in vitro endothelial linings grown within microfluidic channels. Tissue Eng. Part A *17*, 2965–2971.
30. Liu, M., Wu, A., Liu, J., Zhao, Y., Dong, X., Sun, T., Shi, Q., and Wang, H. (2024). TPP-Based Microfluidic Chip Design and Fabrication Method for Optimized Nerve Cells Directed Growth. Cyborg Bionic Syst. *5*, 0095.
31. Schreiner, W., Karch, R., Neumann, M., Neumann, F., Roedler, S.M., and Heinze, G. (2003). Heterogeneous perfusion is a consequence of uniform shear stress in optimized arterial tree models. J. Theor. Biol. *220*, 285–301.
32. Chandran, K.B. (1993). Flow dynamics in the human aorta. J. Biomech. Eng. *115*, 611–616.
33. Naili, S., and Ribreau, C. (1999). Wall shear stress in collapsed tubes. Eur. Phys. J. AP. *5*, 95–100.
34. Weinberg, E.J., Borenstein, J.T., Kaazempur-Mofrad, M.R., Orrick, B., and Vacanti, J.P. (2004). Design and Fabrication of a Constant Shear Microfluidic Network for Tissue Engineering. MRS Proc. *823*, W9.
35. Sonmez, U.M., Cheng, Y.W., Watkins, S.C., Roman, B.L., and Davidson, L.A. (2020). Endothelial cell polarization and orientation to flow in a novel microfluidic multimodal shear stress generator. Lab Chip *20*, 4373–4390.
36. Weinberg, E.J., Borenstein, J.T., Kaazempur-Mofrad, M.R., Orrick, B., and Vacanti, J. (2004). Design and fabrication of a constant shear microfluidic network for tissue engineering. MRS Proc. *820*, 120–125.
37. Nakayama, K.H., Surya, V.N., Gole, M., Walker, T.W., Yang, W., Lai, E.S., Ostrowski, M.A., Fuller, G.G., Dunn, A.R., and Huang, N.F. (2016). Nanoscale Patterning of Extracellular Matrix Alters Endothelial Function under Shear Stress. Nano Lett. *16*, 410–419.
38. Böhm, U.L., Prendergast, A., Djenoune, L., Nunes Figueiredo, S., Gomez, J., Stokes, C., Kaiser, S., Suster, M., Kawakami, K., Charpentier, M., et al. (2016). CSF-contacting neurons regulate locomotion by relaying mechanical stimuli to spinal circuits. Nat. Commun. *7*, 10866.
39. Hubbard, J.M., Böhm, U.L., Prendergast, A., Tseng, P.E.B., Newman, M., Stokes, C., and Wyart, C. (2016). Intraspinal sensory neurons provide powerful inhibition to motor circuits ensuring postural control during locomotion. Curr. Biol. *26*, 2841–2853.
40. He, Y., Qiu, J., Fu, J., Zhang, J., Ren, Y., and Liu, A. (2015). Printing 3D microfluidic chips with a 3D sugar printer. Microfluid. Nanofluidics *19*, 447–456.
41. Qiu, J., Li, J., Guo, Z., Zhang, Y., Nie, B., Qi, G., Zhang, X., Zhang, J., and Wei, R. (2023). 3D Printing of Individualized Microfluidic Chips with DLP-Based Printer. Materials *16*, 6984.
42. Yeh, C.H., Tsai, S.H., Wu, L.W., and Lin, Y.C. (2011). Using a co-culture microsystem for cell migration under fluid shear stress. Lab Chip *11*, 2583–2590.
43. Shin, H.S., Kim, H.J., Sim, S.J., and Jeon, N.L. (2009). Shear stress effect on transfection of neurons cultured in microfluidic devices. J. Nanosci. Nanotechnol. *9*, 7330–7335.
44. Espina, J.A., Cordeiro, M.H., Milivojevic, M., Pajić-Lijaković, I., and Barriga, E.H. (2023). Response of cells and tissues to shear stress. J. Cell Sci. *136*, jcs260985.
45. Chen, I.J., Eckstein, E.C., and Lindner, E. (2009). Computation of transient flow rates in passive pumping micro-fluidic systems. Lab Chip *9*, 107–114.
46. Renault, R., Sukenik, N., Descroix, S., Malaquin, L., Viovy, J.L., Peyrin, J.M., Bottani, S., Monceau, P., Moses, E., and Vignes, M. (2015). Combining microfluidics, optogenetics and calcium imaging to study neuronal communication in vitro. PLoS One *10*, e0120680.
47. Zhang, X., Huk, D.J., Wang, Q., Lincoln, J., and Zhao, Y. (2014). A microfluidic shear device that accommodates parallel high and low stress zones within the same culturing chamber. Biomicrofluidics *8*, 054106.
48. Tang, X., Wang, Z., Khutsishvili, D., Cheng, Y., Wang, J., Tang, J., and Ma, S. (2023). Volumetric compression by heterogeneous scaffold embedding promotes cerebral organoid maturation and does not impede growth. Cell Syst. *14*, 872–882.e3.
49. Loverde, J.R., and Pfister, B.J. (2015). Developmental axon stretch stimulates neuron growth while maintaining normal electrical activity, intracellular calcium flux, and somatic morphology. Front. Cell. Neurosci. *9*, 308.
50. Pfister, B.J., Iwata, A., Meaney, D.F., and Smith, D.H. (2004). Extreme stretch growth of integrated axons. J. Neurosci. *24*, 7978–7983.
51. Athamneh, A.I.M., and Suter, D.M. (2015). Quantifying mechanical force in axonal growth and guidance. Front. Cell. Neurosci. *9*, 359.
52. Sana Ullah Sahar, M., Mettyas, T., Shah, M., Bindra, R., and Barton, M. (2022). Histological, immunohistochemical, and morphometric analysis of negative pressure-assisted in-vivo nerve stretch-growth. Neurosci. Lett. *782*, 136687.
53. Stiess, M., and Bradke, F. (2011). Neuronal polarization: the cytoskeleton leads the way. Dev. Neurobiol. *71*, 430–444.
54. Lowery, L.A., and Van Vactor, D. (2009). The trip of the tip: Understanding the growth cone machinery. Nat. Rev. Mol. Cell Biol. *10*, 332–343.
55. Zhao, S., Suciu, A., Ziegler, T., Moore, J.E., Jr., Bürki, E., Meister, J.J., and

Brunner, H.R. (1995). Synergistic effects of fluid shear stress and cyclic circumferential stretch on vascular endothelial cell morphology and cytoskeleton. Arterioscler. Thromb. Vasc. Biol. *15*, 1781–1786.

56. Yamada, S., Yassin, M.A., Torelli, F., Hansmann, J., Green, J.B.A., Schwarz, T., and Mustafa, K. (2023). Unique osteogenic profile of bone marrow stem cells stimulated in perfusion bioreactor is Rho-ROCK-mediated contractility dependent. Bioeng. Transl. Med. *8*, e10509.
57. Tzima, E., del Pozo, M.A., Shattil, S.J., Chien, S., and Schwartz, M.A. (2001). Activation of integrins in endothelial cells by fluid shear stress mediates Rho-dependent cytoskeletal alignment. EMBO J. *20*, 4639–4647.
58. Yang, H., Guan, L., Li, S., Jiang, Y., Xiong, N., Li, L., Wu, C., Zeng, H., and Liu, Y. (2016). Mechanosensitive caveolin-1 activation-induced PI3K/Akt/mTOR signaling pathway promotes breast cancer motility, invadopodia formation and metastasis in vivo. Oncotarget *7*, 16227–16247.
59. Liu, L., Zong, C., Li, B., Shen, D., Tang, Z., Chen, J., Zheng, Q., Tong, X., Gao, C., and Wang, J. (2014). The interaction between β1 integrins and ERK1/2 in osteogenic differentiation of human mesenchymal stem cells under fluid shear stress modelled by a perfusion system. J. Tissue Eng. Regen. Med. *8*, 85–96.

STAR★METHODS

KEY RESOURCES TABLE

REAGENT or RESOURCE	SOURCE	IDENTIFIER
Antibodies		
Mouse anti-βIII-tubulin	Abcam	Cat. #ab78078; RRID:AB_2256751
Rabbit Anti-MAP2	Abcam	Cat. #ab32454; RRID:AB_776174
Rabbit Anti-GFAP	Abcam	Cat. #ab68428; RRID:AB_1209224
Goat Anti-Mouse IgG H&L (Alexa Fluor® 488)	Abcam	Cat. #ab150113; RRID:AB_2576208
Goat Anti-Rabbit IgG H&L (Alexa Fluor® 647)	Abcam	Cat. #ab150079; RRID:AB_2722623
Chemicals, peptides, and recombinant proteins		
Neurobasal-A medium	Gibco	Cat. #10888022
B27	Gibco	Cat. #17504044
L-glutamine	Gibco	Cat. #A2916801
Glucose	Solarbio	Cat. #G8150
Penicillin/streptomycin	Solarbio	Cat. #P1400
Poly-L-lysine	Solarbio	Cat. #P8130
Collagen type I rat tail	Solarbio	Cat. #C8062
Hoechst 33258	Sigma-Aldrich	Cat. #94403
Experimental models: Organisms/strains		
Sprague-Dawley rat	SiPeiFu Inc.	N/A
Software and algorithms		
SigmaPlot	Systat Software Inc.	Grafiti LLC
Fiji	NIH Image	Fiji (imagej.net)
Other		
Sylgard 184	Dow Corning	SYLGARD™ 184 Silicone Elastomer Kit | Dow Inc.

EXPERIMENTAL MODEL AND STUDY PARTICIPANT DETAILS

Neuron culture and maintenance

In all experiments, the PCNs used were directly isolated from the cortical regions of neonatal male (n = 3) and female (n = 3) Sprague-Dawley rats (P0) (SiPeiFu, Peking, China). All animal experiments agreed with the Guide for the Care and Use of Laboratory Animals and were approved by Beijing Institute of Technology Medical and Experimental Animal Ethics Committee (no. BIT-EC-SCXK 2021-0013-R-131). 20 μL of the cell suspension was seeded into the soma chamber and then placed in an incubator at 37°C with 5% CO2. After 4 h, the neurons were fully adhered. The adhesion medium was removed, 220 μL and 160 μL of maintenance medium were added to the soma and axon chambers, respectively, and the culture was continued in the incubator. The medium was replaced every 3 days. The maintenance medium (50 mL) consisted of neurobasal-A basic medium (Gibco, Gaithersburg, MD, USA), 2% B27 supplement (Gibco, Gaithersburg, MD, USA), 1 mM L-glutamine (Gibco, Gaithersburg, MD, USA), 60 mg/mL glucose (Solarbio, Peking, China), and 1% penicillin/streptomycin (Solarbio, Peking, China). Before seeding, the MCs were coated at room temperature with poly-L-lysine (PLL, Solarbio, Peking, China) for 2 h, followed by an overnight coating at 4°C with collagen type I rat tail (Solarbio, Peking, China) to promote neuronal adhesion.

METHOD DETAILS

Preparation of the microfluidic chips with AMCs

In this study, AMC chips and RMC chips were fabricated via TPP printing (Photonic Professional GT2, Nanoscribe) combined with soft lithography, as shown in Figure S2. The chips used were composed of PDMS blocks with AMCs and dishes. The PDMS blocks contained four cylindrical fluid reservoirs (height: 7 mm, diameter: 6 mm, spacing: 50 μm), a soma chamber, an axon chamber (height: 100 μm, length: 6 mm, width: 1.5 mm), and 120 AMCs (height: 3 μm, diameter: 6 μm, spacing: 50 μm) or RMCs (height: 3 μm, width: 6 μm, spacing: 50 μm). The AMCs and RMCs are the main functional areas where the axons are induced to grow.

DHM system

To characterize the inner surface of the MCs, this study employed the off-axis digital holography technique based on a classic off-axis DHM system. The system mainly consisted of beam expander optics, projection optics, and a CCD, as shown in Figure S3. The beam is collimated by an SF and split into reference and object beams by a BS. The reference beam does not pass through the object itself, while the object beam is focused on the microfluidic chip on the sample stage using an afocal configuration. After the two beams converge at the BS, a hologram containing the thickness information of the MCs is formed and captured by the CCD. This hologram was then processed through holographic phase reconstruction to obtain the thickness matrix of the MCs, as shown in Figure S4. When the beam passes perpendicularly through the MCs, the phase values in the corresponding regions of the hologram change, thus acquiring thickness information of different shapes inside the MCs. The local thickness is mapped one-to-one with the holographic phase. Based on the reconstructed phase information, the high-resolution three-dimensional shape and phase information of the MC surface could be noninvasively reconstructed.

Simulation analysis

To characterize the complex fluidic environment within MCs, the distribution of directed flow in an MC was simulated. Since the pressures at both ends of each MC are the same, only one MC is displayed for analysis. The MC was 3D modeled using SolidWorks software and imported into simulation software. The fluid is considered incompressible, and the flow is laminar. The geometry is fixed in the y-z direction, with a pressure gradient along the x axis acting at the inlet of the MC.

Immunofluorescence staining

The cultures were fixed in 4% paraformaldehyde for 15 min and permeabilized with 0.3% Triton X-100 in PBS for 10 min. The cultures were blocked with 10% BSA in PBS for 30 min, and incubated overnight at 4°C with primary antibodies. The primary antibodies used included βIII tubulin (mouse, Abcam, ab78078, 1:250), MAP-2 (rabbit, Abcam, ab32454, 1:250) and GFAP (rabbit, Abcam, ab68428, 1:400). Subsequently, the samples were incubated with secondary antibodies (Alexa Fluor 488 or 647, Abcam, 1:1000) in the dark at room temperature for 2 h. The neuronal nuclei were counterstained with Hoechst 33258 (Sigma-Aldrich, St. Louis, MO, USA, 1:500) for 10 min, and observed under a confocal microscope.

QUANTIFICATION AND STATISTICAL ANALYSIS

Axonal growth was monitored by scanning AMC chips and RMC chips with cultured PCNs under a confocal microscope (A1, Nikon, Japan). Immunostaining images were quantified with Fiji software. To quantify axonal length, 2D skeletonization analysis of immunofluorescence images was performed using the AnalyzeSkeleton function of Fiji, as shown in Figure S5. The pixels of axons at the inlets and outlets of the MC in the skeleton image were marked and connected, and their average length and offset angle relative to the chamber edge were finally measured. The data are expressed as the mean ± standard deviation (SD) and were analyzed using SigmaPlot software. Statistical comparisons between the parallel groups were analyzed by one-way ANOVA. Significance levels are indicated as follows: $*p < 0.05$; $**p < 0.01$; $***p < 0.001$. The sample sizes are indicated in the figure legends. All experiments were performed with $n = 3$ or greater.